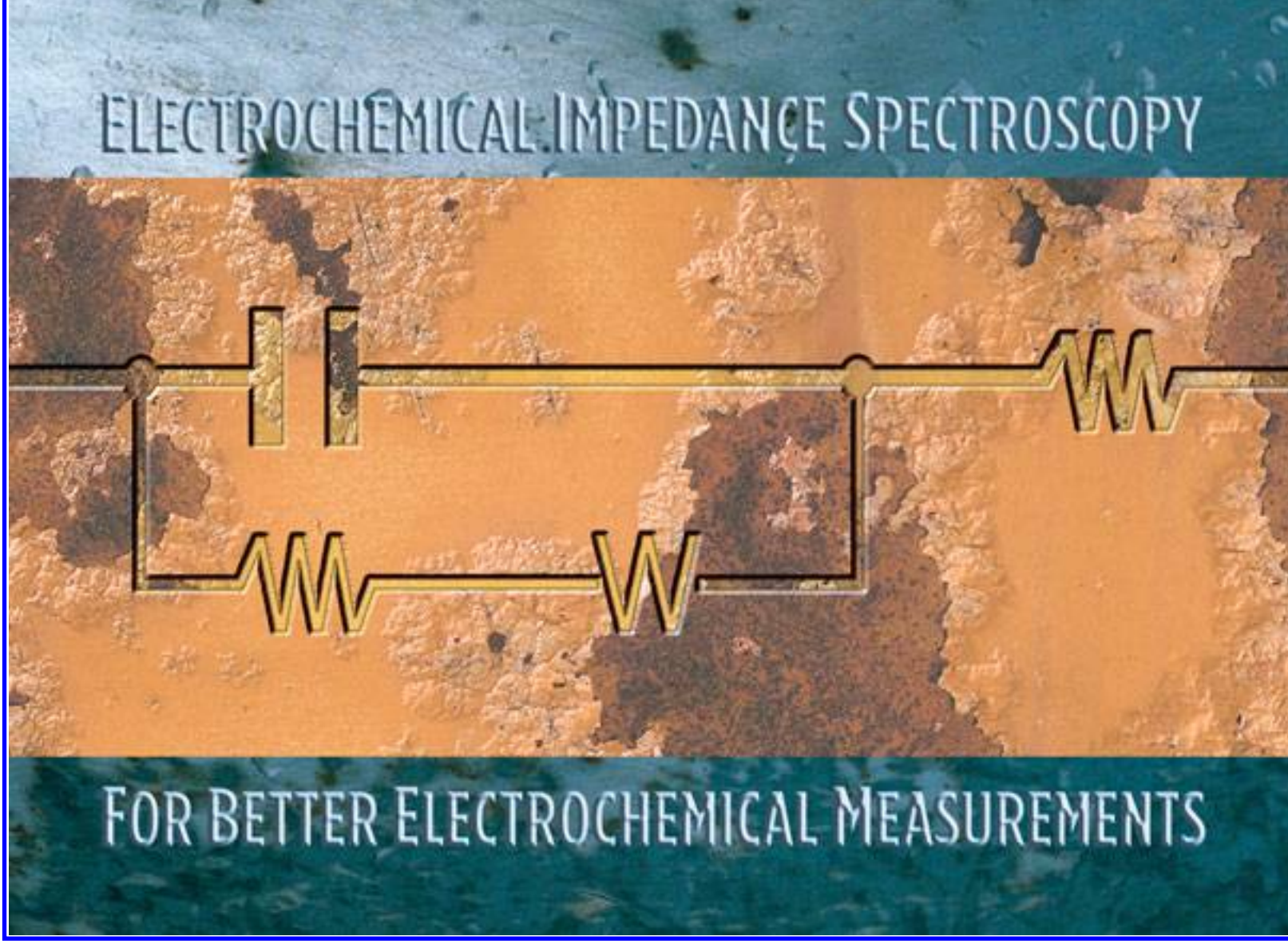

With impedance data, a complete description of an electrochemical system is possible.

An electrochemical reaction at the electrode–electrolyte interface cannot be fully understood by using traditional electrochemical measurements. Those methods provide only currents made of faradaic and nonfaradaic components. A complete description requires impedance measurements made over a broad frequency range at various potentials and determination of all the electrical characteristics of the interface, which can be thought of as a thin capacitor that forms between the charged electrode and the counter ions lined up parallel to it (*1*, *2*). In this article, we will explain how a simple interface is described by an equivalent circuit, how the electrochemical reaction rates are better understood using electrochemical impedance spectroscopy (EIS), how the electronic components of the circuit are determined by impedance measurements, and applications of EIS.

Representations of the electrified interface have gradually evolved from repeated modifications (Figure 1a) of the model first proposed by Helmholtz (*3*). In a simple case, the interface can be modeled by an equivalent circuit (Figure 1b), also called a Randles circuit (*4*), made of a double-layer capacitor in parallel with a polarization resistor (also known as a charge-transfer resistor with certain constraints) and a Warburg impedance, connected in series with a resistor that measures the resistance of the electrolyte solution. Depending on the types of electrochemical reactions involved at the interface, the equivalent circuit can be much more complicated.

The model in Figure 1b predicts that a faradaic current, which is due to the redox reactions, is always coupled with a capacitive component. Capacitance is regarded as noise, and considerable efforts have been made to eliminate or minimize it, resulting in tast (sampling), normal pulse, and differential pulse voltammetry (*1*). However, reducing or minimizing the effects of nonfaradaic currents is considered a passive way to solve the problem. A more active and direct approach would be to determine and separate the faradaic currents from the nonfaradaic signals (*5*), which is possible with EIS because it provides all the information about the interface and the electrolyte solution. Removing the noise and reconstructing the voltammograms of only the faradaic currents may solve another problem of traditional voltammetric measure-

Su-Moon Park • Jung-Suk Yoo Pohang University of Science and Technology (Korea)

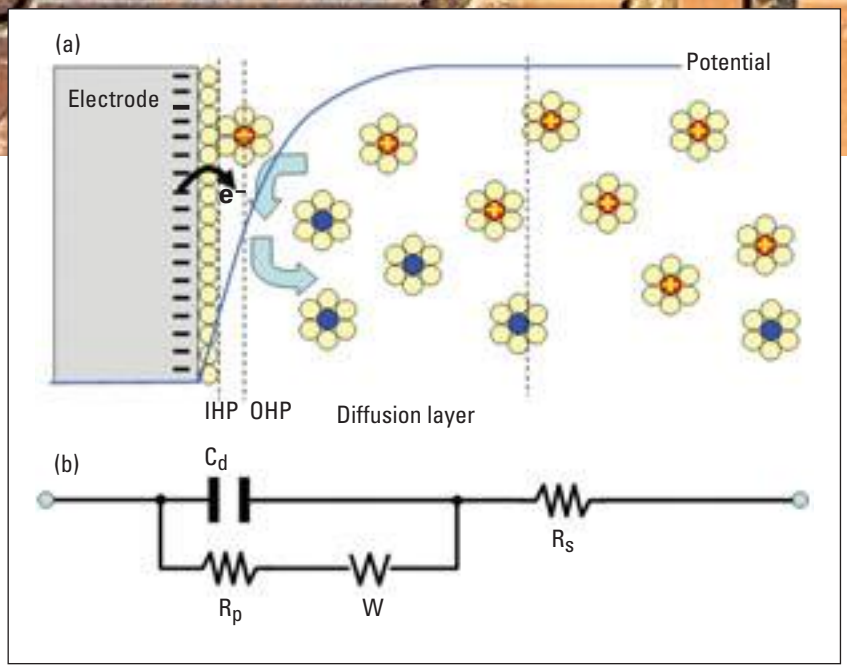

FIGURE 1. A simple electrified interface, in which the vertical dotted lines in (a) are represented by the electronic components in (b).

(a) The oxidants (red) with a positive charge diffuse toward the negatively charged electrode, accept electrons from the electrode at the interface, become the reductants (blue), and diffuse to the bulk of the solution. The oxidant is also a counterion to the electrode. No specific adsorption is considered at the interface. IHP and OHP are the inner and outer Helmholtz planes, respectively. (b) An equivalent circuit representing each component at the interface and in the solution during an electrochemical reaction is shown for comparison with the physical components. C_d, double layer capacitor; R_p, polarization resistor; W, Warburg resistor; R_s, solution resistor.

ments—the need to improve sensitivity, which is commonly addressed by stripping voltammetry.

What is impedance?

Impedance is a totally complex resistance encountered when a current flows through a circuit made of resistors, capacitors, or inductors, or any combination of these. Depending on how the electronic components are configured, both the magnitude and the phase shift of an ac can be determined. Because an inductive effect is not usually encountered in electrochemistry, we consider only the simple equivalent circuit shown in Figure 1b in which no inductor is present.

However, first consider an experiment in which a series of increasing dc potentials (a ramp) are applied to a working electrode in an electrochemical cell containing an electroactive species. A current–potential curve (Figure 2) is obtained, which is described by the Butler–Volmer equation (solid line)

$$i = i_0 \left[e^{\frac{-\alpha n F}{RT}\eta} - e^{\frac{(1-\alpha) n F}{RT}\eta} \right] \qquad (1)$$

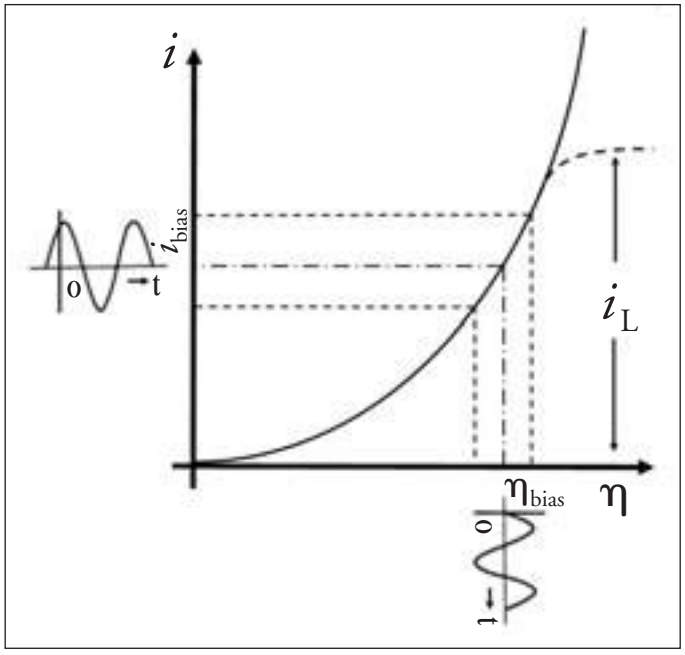

FIGURE 2. The dc plotted as a function of overpotential according to the Butler–Volmer equation (solid line), which is limited by mass transport at large overpotentials (dashed line curving to the right), an ac voltage (broken line) superimposed on the dc bias potential, η_{bias} (dot-dashed line), shown on the i axis [$\eta_{bias} + \Delta\eta\sin(\omega t)$], and the resulting ac superimposed on the dc on the i axis [$i_{bias} + \Delta i\sin(\omega t + \phi)$]. R_p is obtained by taking $\Delta\eta/\Delta i$, in which i is obtained after applying the ac voltage wave at a given η.

in which η is the overpotential defined as $E - E_{eq}$, with E and E_{eq} representing the applied and equilibrium potentials, respectively; i_0 is the exchange current at $\eta = 0$; n is the number of electrons transferred; F is the Faraday constant; R is the gas constant; T is the absolute temperature; and α is the transfer coefficient for electron transfer. The faradaic current i is limited by the mass transport (dashed line curving to the right) when the rate of electron transfer becomes large enough. At a given overpotential η_{bias}, the slope of the curves, $di/d\eta_{bias}$, is $1/R_p$, in which R_p is the polarization resistance. When a small ac voltage wave of frequency ω at η_{bias} (Figure 2) is superimposed, the ac of the same frequency will be flowing on top of the dc. Because the interface has resistors and a capacitor (Figure 1b), the flowing ac will experience a phase shift, expressed as i_{bias}, caused by the ac wave perturbation.

For an equivalent circuit (Figure 1b), a straightforward impedance expression can be derived by applying Ohm's law to two components connected in parallel. One of these is R_p, and the other is $1/(j\omega C_d)$, in which C_d is the double-layer capacitance.

$$Z(\omega) = R_s + \frac{R_p}{1 + j\omega R_p C_d} = R_s + \frac{R_p}{1 + \omega^2 R_p^2 C_d^2} - \frac{j\omega R_p^2 C_d}{1 + \omega^2 R_p^2 C_d^2} = Z' + jZ'' \qquad (2)$$

To make the derivation of the equation and its interpretation straightforward, we neglected the contribution of the Warburg component. Thus, the impedance of the interface consists of two parts, a real number Z' and an imaginary number Z'' with a com-

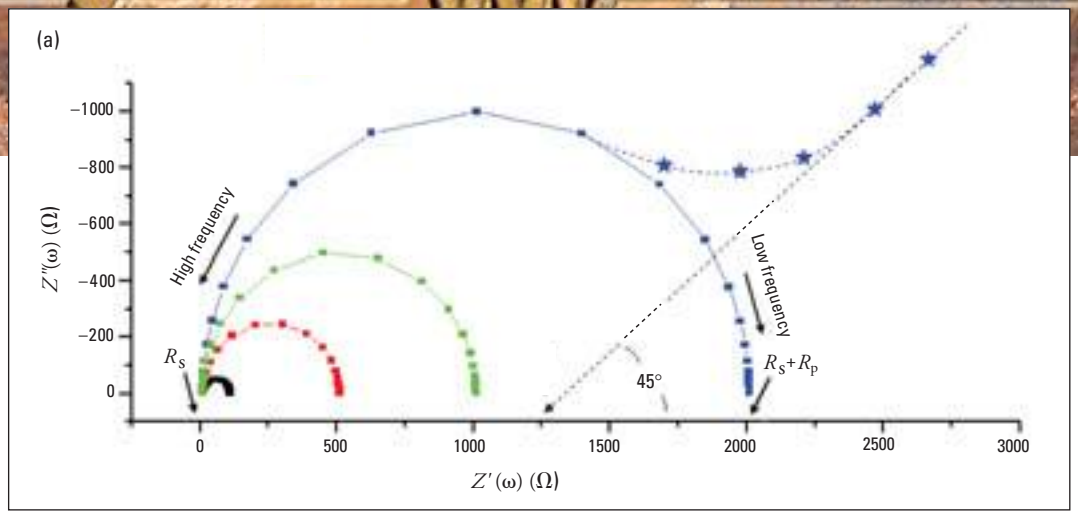

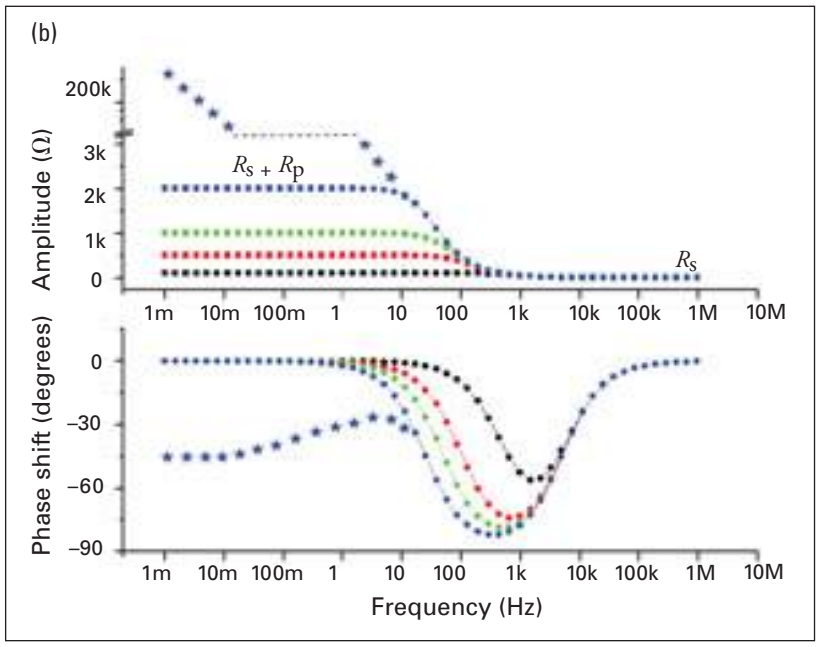

FIGURE 3. (a) Nyquist and (b) Bode plots.

The data shown here, which were computer-generated using Eq. 4 from arbitrarily picked values of R_p, represent the impedance results regardless of the measurement methods used. Plots of real data obtained by DTFT can be found in Refs. 32 and 52. The contribution from the Warburg impedance (blue stars) is shown only for one case (R_p = 2 kΩ) for both plots. (b, top) The amplitude axis is in logarithmic scale at amplitudes >3 kΩ in the amplitude vs frequency plot to accommodate the large Warburg impedance values. Note that the phase angle in both (a) and (b) approaches 45° as the Warburg contribution becomes dominant. The black dashed line in (a) represents Warburg components with its intercept at $R_s + R_p - R_p^2\lambda^2 C_d^2$, from which λ = 3.08 is obtained; therefore, $k_f = 4.1 \times 10^{-3}$ cm/s for a diffusion coefficient of 1.8×10^{-6} cm^2/s. R_s, 10 Ω; C_d, 20 μF; R_p black, 100 Ω; R_p red, 500 Ω; R_p green, 1 kΩ; R_p blue, 2 kΩ.

tum states in spectroscopic transitions.

By treating the impedance data in such a frequency range, system characteristics for an electrochemical reaction (i.e., R_s, R_p, and C_d) can be obtained. R_p is a function of potential; however, at η = 0, it becomes the charge-transfer resistance R_{CT}. Two convenient ways of treating the impedance data are the Nyquist plot, in which imaginary numbers $Z''(\omega)$ are plotted against real numbers $Z'(\omega)$, and the Bode plot, in which absolute values of impedance or phase angle are plotted against the frequency.

Extraction of the system characteristics requires interpreting the Nyquist plot (Figure 3a) according to Equation 2. At high frequencies, the frequency-dependent term of Equation 2 vanishes, resulting in $Z(\omega) = Z'(\omega) = R_s$, which is an intercept on the $Z'(\omega)$ axis on the high-frequency side ($\phi = 0$ or $Z''(\omega) = 0$). For $\omega \rightarrow 0$, Equation 2 becomes $Z(\omega) = R_s + R_p$, which is an intercept on the $Z'(\omega)$ axis on the low-frequency side. At the frequency where a maximum $Z''(\omega)$ is observed, the straightforward relationship $R_p \cdot C_d = 1/\omega_{max} = 1/(2\pi f_{max}) = \tau_{rxn}$, which is the time constant of the electrochemical reaction, can be shown and indicates how fast the reaction takes place. Also, if $R_p \cdot C_d$ is known, C_d can be obtained because R_p is already known from the low-frequency intercept on the $Z'(\omega)$ axis. The Nyquist plot gives all the necessary information about the electrode–electrolyte interface and the reaction.

Similar information is obtained by examining the Bode diagram (Figure 3b) using Equation 2. Log R_s and log (R_p+R_s) are obtained straightforwardly from the $Z(\omega)$ versus log ω plot at high and low frequencies from the same argument as the Nyquist plot. In the intermediate frequency region, an almost straight line with a slope of ~–1.0 can be seen. The equation for this line is obtained by ignoring the frequency-independent terms, R_s and 1 in the denominator, of Equation 2 to yield

$$Z(\omega) = R_s + \frac{R_p}{1+j\omega R_p C_d} \qquad (3)$$

Taking the logarithm on both sides of the resulting equation yields log $Z(\omega)$ = –log ω – log C_d, which says that log $|Z(\omega)|$ versus log ω would have a slope of –1, and C_d can be obtained from the intercept of this line with the $Z(\omega)$ axis when –log ω = 0 at ω = 1. Thus, the Bode plot provides the same information

plex representation, $Z(\omega) = Z'(\omega) + jZ''(\omega)$ with ϕ (the phase angle) = $\tan^{-1}[Z''(\omega)/Z'(\omega)]$. Although the capacitance is relatively constant over the potential at a given electrode, the R_p varies as a function of η_{bias} applied to the electrode.

At a given dc bias potential, a series of $Z(\omega)$ data are obtained in a range of frequencies, typically 100 kHz–1×10^{-4} Hz. The impedance varies, depending on frequencies, and is often plotted in different ways as a function of frequency (making it a spectroscopic technique), hence, the name EIS (*1*, *6*). However, this is a misnomer because the frequencies do not represent energy levels and thus the impedance has nothing to do with quan-

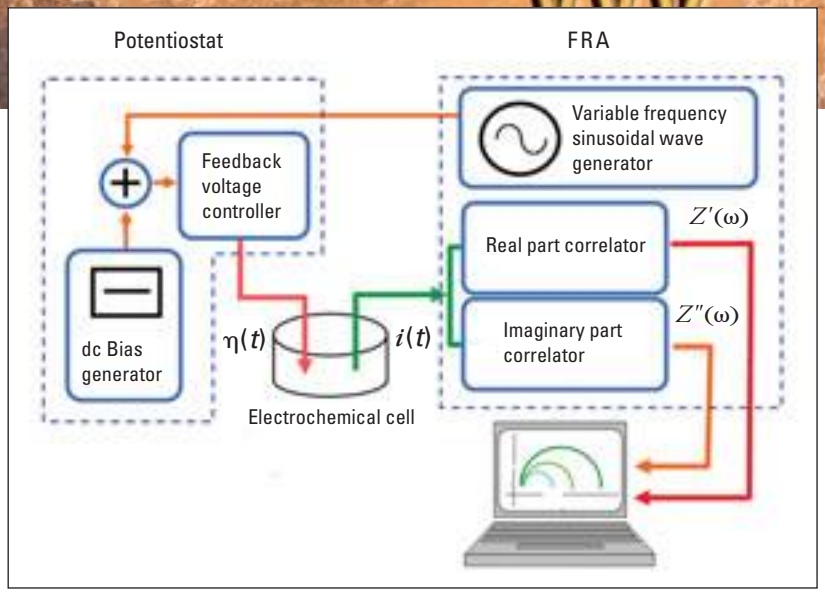

FIGURE 4. Concept of the frequency response analyzer (FRA).

as the Nyquist plot. The ϕ versus log ω plot shows that the impedance responses are resistive primarily at high and low frequencies as indicated by practically no phase shifts, whereas at intermediate frequencies, they are mostly capacitive as their phase shifts get closer to 90°.

Thus far, we have discussed the equivalent circuit without considering the effect of the Warburg impedance; however, its contribution can be important at low frequencies because the mass transport of the electroactive species may limit the electron-transfer process. The Warburg impedance (*7*) is imparted by mass transfer and can be derived by

$$Z(\omega) = R_s + R_p\left[1+\frac{\lambda}{\sqrt{2\omega}}\right] - R_p^2\lambda^2 C_d - \frac{jR_p\lambda}{\sqrt{2\omega}} \qquad (4)$$

in which $\lambda = k_f/\sqrt{D_O} + k_b/\sqrt{D_R}$, and k_f and k_b are the forward and backward electron-transfer rate constants, respectively, and D_O and D_R are the diffusion coefficients for the oxidant O and the reductant R, respectively, for the reaction $O + ne^- \leftrightarrow R$. Here the frequency-dependent terms $\lambda/\sqrt{2\omega}$, appearing in both the real and the imaginary terms in Equation 4, are called the Warburg impedance. When $Z''(\omega)$ is plotted against $Z'(\omega)$ with the Warburg component included, the high- and low-frequency intercepts on the $Z'(\omega)$ axis are still R_s and $R_s + R_p$, as was the case without the Warburg impedance, and the plot of the Warburg components becomes a straight line with a slope of unity and an intercept of $R_s + R_p - R_p^2\lambda^2 C_d$ (black dashed line in Figure 3a). Thus we can calculate λ, and thereby the diffusion coefficient from λ when k_f is known, and k_f can be obtained from $i_f = nFAk_fC_O$, in which C_O is the bulk concentration of oxidant and A is the area. In other words, we now have a complete description of the electrochemical system.

Measuring impedance

The principle shown in Figure 2 is the basis on which impedance is measured: A small ac wave, typically 5–10 mV (peak-to-peak) of a given frequency, is superimposed on the dc η_{bias}, and the resulting ac and its phase shift i_{bias} are measured. These measurements may be made in various ways (*8–10*); however, the frequency response analyzer (FRA; Figure 4) has become the industry standard in electrochemical instrumentation in recent years. The reference ac wave of frequency ω superimposed on a given dc bias potential is applied to a working electrode in the electrochemical cell. The ac signal $S(t)$ obtained from the cell is then multiplied by the reference sine or cosine wave and integrated to obtain

$$Z'(\omega) = \frac{1}{NT}\int_0^{NT} S(t) \cdot \cos(\omega t)\,dt \qquad (5)$$

and

$$Z''(\omega) = \frac{1}{NT}\int_0^{NT} S(t) \cdot \sin(\omega t)\,dt \qquad (6)$$

Here T is the period $(1/f)$ of the ac wave, N is the number of cycles included in the integration, and $\sin(\omega t)$ and $\cos(\omega t)$ are the reference signals. Higher harmonics that crept in during the operations are removed by digital filtering. As in any other measurements, the S/N is enhanced by $N^{1/2}$, in which N is the number of cycles included in the integration.

Although the FRA is state of the art, it has a few shortcomings. The entire frequency range must be scanned by generating ac voltage waves of 10–20 representative frequencies per decade to make measurements. Often, measurements of more than a few ac cycles are necessary at a given frequency to obtain a decent S/N, and the instrument usually waits for the system to reach a constant (or equilibrium) current after a step to a desired dc bias potential before it takes measurements. Thus, this method is viable only for an electrochemically stable system in equilibrium. All these operations often take longer than they should, and the system can change significantly by the time the measurements are made, particularly when the electrochemical reaction is not reversible or involves a series of subsequent reactions such as adsorption–desorption and/or deposition–dissolution processes after the initial electron transfer.

To overcome these problems, investigators have proposed several improvements, such as software corrections after the measurements have been taken or new measurement principles. Early investigators questioned the validity of impedance measurements (*11*, *12*) and postulated that instantaneous impedance measurements of the nonstationary systems were needed because traditional methods provide impedance data only for the stationary systems. Stoynov et al. presented some mathematical expressions to extract instantaneous impedance values for nonstationary systems from the results obtained on stationary systems (*13–16*). Macdonald et al. also presented requirements for "true" impedance signals; the stability and linearity of a system can be demonstrated only when imaginary and real components are interconvertible via Kramers–Kronig transforms (*17*).

To reduce the impedance measurement time, many investigators have proposed techniques in which no frequency scanning

is used. Smith et al. and others suggested using fast FT (FFT) for impedance measurements (*18–27*). Popkirov and Schindler recently incorporated Smith's multiwave FFT method into an electrochemical impedance spectrometer in which ac waves of 42 properly selected frequencies are mixed and the resulting voltage signal is applied to an electrochemical system on top of the dc bias voltage (*28*). The current signal obtained in the time domain is then converted back into ac signals in the frequency domain by FFT operations.

Pilla reported a "transient impedance technique" in which the time domain response of an arbitrary perturbation was converted to the data in the frequency domain using a Laplace transform; Smyrl published a similar approach (*29*, *30*). Barsoukov et al. recently incorporated this technique into an electrochemical impedance spectrometer by using a variety of excitation signals such as current step, voltage step, current interrupt, and others (*31*). One vendor's instrument made high-frequency measurements first with the FRA, and then the multiwave FFT method took over when the frequency went below a certain limit. Although the combined method saved some time by making measurements over a wide frequency range, it took as long to measure the slowest signal as it did to measure the entire range. Besides, discontinuities in impedance spectra are often observed when the measurement method is switched over.

A recent notable development takes advantage of the fact that the sum of ac waves of all frequencies, rather than properly selected frequencies, is an impulse signal called a Dirac δ function (*32–36*). The properties of the Dirac δ function are as follows: $\delta(t) = 0$ for $t \neq 0$; $\delta(t)$ is undefined for $t = 0$; and $\int\delta(t)dt = 1$ from 0 to $-\infty$. These properties state that the function has a δ shape with a base of almost 0 and an infinitely large height. Thus, an application of the Dirac δ function to an electrochemical system is equivalent to applying the ac waves of all frequencies with an identical phase at the same time. The dc thus obtained is a composite signal of ac of all frequencies, which can be transformed to that of each frequency using the discrete time FT (DTFT) multiwave formalism. This converts the data in the discrete time domain to the continuous frequency domain. Although this approach appears simple, it would be very hard, if not impossible, to actually apply it to an electrochemical system. Generating a Dirac δ function (impulse) by a known electronic device is difficult, and applying the impulse signal to an electrochemical cell may damage the system.

One way to get around this problem is to take advantage of a theorem that states, for a linear system, that if an input voltage signal $v(t)$ produces a current signal $i(t)$, it responds with a derivative or integrated current signal $i'(t)$ or $\int i(t)dt$, upon inputting a derivative or integrated voltage signal, $v'(t)$ or $\int v(t)dt$, instead (*36–38*). Thus, the integrated form of the Dirac δ function, which is a voltage step, can be used. However, another problem is that this theorem assumes that the electrochemical system is linear. Electrochemical systems are not linear because the Butler–Volmer equation describes the current. A small step signal can circumvent this problem; the Butler–Volmer equation is often linearized when the change in η is small (*1*). When a part of the system is linearized, it is called a piecewise linear system (*39*). Thus, a small voltage step, 5 or 10 mV, can be used as an excitation signal to meet the linearity stipulation. The first derivative of the current obtained after a small step is applied would then be the same as the current response, had the voltage signal of the Dirac δ function been applied (Figure 5). FT of this signal gives ac signals in the frequency domain of the DTFT multiwave formalism. In short, the derivative signal of the chronoamperometric current would be the signal obtained if the Dirac δ function had been applied, and this signal would contain ac of all frequencies.

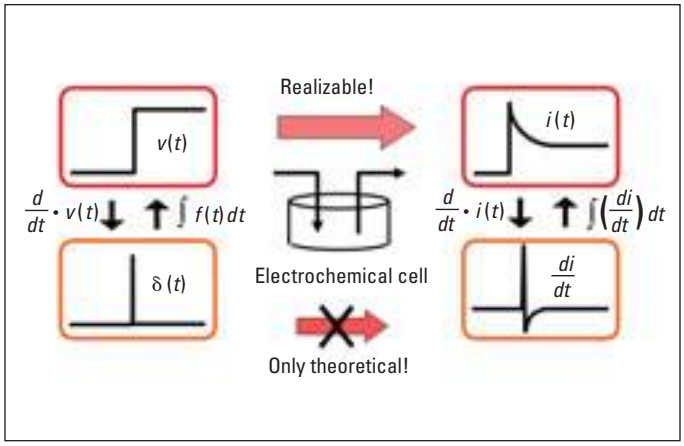

FIGURE 5. Fast impedance method.

Although this sounds simple, a few more requirements must be met. First, the potentiostat must be very fast so that it provides a well-defined step signal. The derivative of the step signal would not be a Dirac δ function unless it were well defined with a fast rise time; step signals with slow rise times contain a large amount of significantly distorted ac waves, particularly at high frequencies. Second, the data acquisition system must have a high bit-resolution and be fast enough not to lose important information included in a short period of the Dirac δ function, which may be a few tens to hundreds of microseconds.

With this approach, a series of impedance data can be obtained in a full-frequency region in a matter of a few milliseconds, including two features not seen in results using conventional methods. First, the Nyquist and Bode plots are almost always ideal, as predicted, because they represent the snapshots of impedance during a short period of the experiment. This situation is rather unusual because the impedance signals acquired by other techniques are hardly ideal (*32*, *40–51*), perhaps because the impedance obtained by the FRA is the time-averaged signal over the period of the measurement. Even for a complex system, such as aniline oxidation leading to the formation of polyaniline, nearly ideal semicircles are observed (*52*). Thus, it appears that true impedance data are acquired by the fast impedance method, which may eventually replace traditional experiments.

Second, the Warburg impedance is missing in the Nyquist plot because the experiment is carried out in such a brief period (*32*), which could be a shortcoming of this technique. It is assumed that the Warburg resistance is included in R_p, which varied depending on the length of the data acquisition period (*52*), because the chronoamperometric currents would be determined by the circuit made of R_s, R_p, and C_d during an early stage after the step. However, the currents would later be limited by the mass transport, following Cottrell behavior. The Cottrell equation considers only the diffusion-controlled faradaic currents, and the currents originating from R_s and C_d are ignored (*1*). The early rise and decay of the chronoamperometric current takes R_s, R_p, and C_d into account during the first few milliseconds after the potential step, making fast impedance measurements possible before the diffusion process becomes important. Thus, the time constant of the potentiostat should be sufficiently small so it does not affect the current rise and decay of the system.

Applications and prospectives

What good are impedance data to electrochemists, and what is the future of the technique? With impedance data, a complete description of an electrochemical system can be made using an equivalent circuit. The Randles circuit can be worked out by fitting the experimentally obtained impedance data to the theoretical behavior of the postulated equivalent circuit; the fitting provides all the related parameters. Several software programs are commercially available for this purpose (e.g., from Solartron, www.solartronanalytical.com, and Princeton Applied Research, www.princetonappliedresearch.com).

Impedance measurements are useful for studying anodic behavior of metals, corrosion, and surfaces of polymer-modified electrodes.

Although impedance responses for a simple system have been described, a few systems can be represented as simply as shown in Figure 1, and thus the actual responses are not always represented by those shown in Figure 3. In many cases, components with properties somewhere between the discrete electronic components—called the constant-phase elements—are needed to describe the impedance behaviors (*6*). As a result, it could be very difficult to simulate the impedance response with discrete components such as a resistor, capacitor, or Warburg impedance. For this reason, many impedance data do not fit the theoretical behavior predicted by the equivalent circuit made of ideally behaving components. For such a system, constant-phase elements are used instead and the resulting interpretations are not always straightforward.

Nonetheless, impedance measurements are most useful for studying complex systems such as anodic behaviors of metals and other composite materials (*40–43*), corrosion (*44*), states of electrodes during charging/discharging cycles of batteries (*45–48*), surface characterization of polymer-modified electrodes (*49–51*), and many other complex electrochemical phenomena. In most complex systems, the impedance responses are made of more than one semicircle. The second or third semicircles in lower frequency domains, when present, represent the electrochemical reactions of slower rise times. When the interface is complex because of adsorption or chemical reactions, more than one semicircle can be observed.

The $i-\eta$ curve (Figure 2) follows the Butler–Volmer equation (solid line) until the current is limited by mass transfer when η becomes large, resulting in a limiting current as shown by the dashed line curving to the right. Although the Nyquist and Bode plots are very useful for extracting various parameters for the electron-transfer reaction, the $i-\eta$ curve constructed from the impedance data can provide information not available from the impedance results alone. The current at a given η can be obtained from

$$i(\eta) = \int \frac{1}{R_p}\, d\eta \qquad (7)$$

and the electrokinetic parameters such as i_0 and α are obtained by fitting the data to Equation 1. With the fast impedance measurement method, the Butler–Volmer region can be pushed to a significantly larger η than in the experiments in which the solution is rigorously stirred. For example, in rotating disk experiments, fast impedance measurements are not limited by mass transport, that is, when η is extended by as much as 250 mV beyond the peak potential of the cyclic voltammogram for oxidation of the ferrocyanide. The current at this potential is ~200× that of the cyclic voltammetry peak. The current beyond the limiting region still follows the Butler–Volmer increase, and thus the current sensitivity increases significantly. This increase not only enhances sensitivity without the interference effects from nonfaradaic currents but also makes it possible to obtain accurate electrokinetic parameters.

Another important application of the fast method is real-time in situ impedance measurement (*52*). The FRA method takes too long to be used for real-time in situ studies, even for a stable system. Most electrochemical systems do not require very fast experiments because of relatively slow rise times ($R_p \cdot C_d$). Thus, real-time in situ experiments would actually reveal the instantaneous impedances of nonstationary electrochemical systems. Preliminary results obtained on the oxidation of aniline are very promising (*52*). Staircase voltammetric experiments of small potential steps were performed, and the current decays in the early part of the experiment were subjected to impedance analysis. Although aniline oxidation is a very complex electrochemical reaction, in which the final oxidation products are formed after a series of electrochemical–chemical reactions and modify the electrode surface continuously (*53*), well-defined impedance re-

sults were obtained. Earlier aniline oxidation studies using traditional methods were much more complex (*50*). The later results indicate that the fast impedance technique does indeed record instantaneous impedance data, whereas traditional techniques record time-averaged results. The fast impedance method is indeed fast enough for the electrochemical reaction timescale.

Impedance measurements have changed the way electrochemists interpret the electrode–electrolyte interface. The technique will offer the most powerful analysis on the status of electrodes during charging–discharging processes of batteries and fuel cells as well as during corrosion experiments. More importantly, this technique may be used to monitor and probe many different processes that occur during electrochemical experiments, including adsorption of reactants and products as well as various reactions that either precede or follow the experiments, thereby changing the electrical characteristics of electrode–electrolyte interfaces.

The fast impedance technique is in a good position to change the way electroanalytical measurements are made and interpreted because noise signals can be rejected. With proper development, sensitivities of electroanalytical techniques may be enhanced by extending the η region such that the currents will not be limited by diffusion. Finally, we hope to soon see multiple hyphenated techniques such as spectroelectrochemical/microgravimetric/impedance measurements during electrochemical experiments.

We gratefully acknowledge the Korea Science and Engineering Foundation for supporting this research through the Center for Integrated Molecular Systems at Pohang University of Science and Technology and the BK-21 program of the Korea Research Foundation for providing graduate stipends to JSY.

Jung-Suk Yoo is a graduate research assistant, and Su-Moon Park is a professor at the Pohang University of Science and Technology. Yoo's research interests include electrochemical instrumentation. Park's research interests include electrochemical instrumentation, nanoscopic studies of and reactions at electrode–electrolyte interfaces, electrochemical and spectroscopic studies of conducting polymers, and materials chemistry, using electrochemical and scanning probe microscopic techniques. Address correspondence to Park at Department of Chemistry, Pohang University of Science and Technology, Pohang, Gyeongbuk 790-784, S. Korea (smpark@postech.edu).

References

(1) Bard, A. J.; Faulkner, L. R. *Electrochemical Methods*; Wiley & Sons: New York, 2001; Chapters 3, 5, 7, 10, 13.
(2) Schmickler, W. *Interfacial Electrochemistry*; Oxford University Press: Oxford, 1996.
(3) Parsons, R. *Chem. Rev.* **1990**, *90*, 813.
(4) Randles, J. E. B. *Trans. Faraday Soc.* **1948**, *44*, 327.
(5) Pankaj, S.; et al. *Anal. Chem.* **1997**, *69*, 1662.
(6) Macdonald, J. R. *Impedance Spectroscopy*; Wiley/Interscience: New York, 1987.
(7) Sluyters-Rehback, M.; Sluyters, J. H. In *Electroanalytical Chemistry*; Bard, A. J., Ed.; Marcel Dekker: New York, 1970; Vol. 4.
(8) de Levie, R.; Husovsky, A. A. *J. Electroanal. Chem.* **1969**, *20*, 181.
(9) Armstrong, R. D.; Henderson, M. *J. Electroanal. Chem.* **1972**, *40*, 121.
(10) Armstrong, R. D.; Race, W. P.; Thirsk, H. R. *Electrochim. Acta* **1974**, *19*, 215.
(11) Sluyters-Rehbach, M.; Sluyters, J. H. *J. Electroanal. Chem.* **1979**, *102*, 415.
(12) Popkirov, G. S.; Schneider, R. N. *Electrochim. Acta* **1993**, *38*, 861.
(13) Stoynov, Z. B.; Savova-Stoynov, B. S. *J. Electroanal. Chem.* **1985**, *183*, 133.
(14) Savova-Stoynov, B.; Stoynov, Z. B. *Electrochim. Acta* **1992**, *37*, 2353.
(15) Stoynov, Z. *Electrochim. Acta* **1992**, *37*, 2357.
(16) Stoynov, Z. *Electrochim. Acta* **1993**, *38*, 1919.
(17) Urquidi-Macdonald, M.; Real, S.; Macdonald, D. D. *Electrochim. Acta* **1990**, *35*, 1559.
(18) Creason S. C.; Smith, D. E. *J. Electroanal. Chem.* **1972**, *36*, 1.
(19) Creason S. C.; Smith, D. E. *Anal. Chem.* **1973**, *47*, 2401.
(20) Smith, D. E. *Anal. Chem.* **1976**, *48*, 221 A, 517 A.
(21) Schwall, R. J.; et al. *Anal. Chem.* **1977**, *49*, 1797.
(22) Schwall, R. J.; Bond, A. M.; Smith, D. E. *Anal. Chem.* **1977**, *49*, 1805.
(23) O'Halloran, R. J.; Schaar, J. E.; Smith, D. E. *Anal. Chem.* **1978**, *50*, 1073.
(24) Crzeszczuk, M.; Smith, D. E. *J. Electroanal. Chem.* **1983**, *157*, 205.
(25) Bond, A. M. *J. Electroanal. Chem.* **1974**, *50*, 285.
(26) Ühlken, J.; Waser, R.; Wiese, H. *Ber. Bunsen-Ges. Phys. Chem.* **1988**, *92*, 730.
(27) Házī, J.; et al. *J. Electroanal. Chem.* **1997**, *437*, 1.
(28) Popkirov, G. S.; Schindler, R. N. *Rev. Sci. Instrum.* **1992**, *63*, 5366.
(29) Pilla, A. *J. Electrochem. Soc.* **1970**, *117*, 467.
(30) Smyrl, W. *J. Electrochem. Soc.* **1985**, *132*, 1551.
(31) Barsoukov, E.; Ryu, S. H.; Lee, H. *J. Electroanal. Chem.* **2002**, *536*, 109.
(32) Yoo, J.-S.; Park, S.-M. *Anal. Chem.* **2000**, *72*, 2035.
(33) Lasia, A. *Anal. Chem.* **2001**, *73*, 4059.
(34) Yoo, J.-S.; Park, S.-M. *Anal. Chem.* **2001**, *73*, 4060.
(35) Spanier, J.; Oldham, K. B. *An Atlas of Functions*; Hemisphere Publishing Corp.: New York, 1987; Chapter 9.
(36) Gabel, R. A.; Roberts, R. A. *Signals and Linear Systems*; Wiley & Sons: New York, 1987.
(37) Carlson, A. B. *Communication Systems*; McGraw-Hill: Singapore, 1986.
(38) Ifeachor, E. C.; Jervis, B. W. *Digital Signal Processing*; Addison-Wesley: New York, 1993.
(39) Sedra, A. S.; Smith, K. C. *Microelectronic Circuits*; Saunders College Publications: Tokyo, Japan, 1991.
(40) Keddam, M.; Mattos, O. R.; Takenouti, H. J. *J. Electrochem. Soc.* **1981**, *128*, 257, 266.
(41) Schmidt, E.; et al. *Electrochim. Acta* **1986**, *31*, 1041.
(42) Cai, M.; Park, S.-M. *J. Electrochem. Soc.* **1996**, *143,* 2125.
(43) Cha, D. K.; Park, S.-M. *J. Electrochem. Soc.* **1997**, *144*, 2573.
(44) Lay, P.; et al. *J. Appl. Electrochem.* **1985**, *15*, 755.
(45) Karunathilaka, S.A.G.R.; et al. *J. Appl. Electrochem.* **1983**, *13*, 577.
(46) Cha, D. K.; Park, S.-M. *J. Electroanal. Chem.* **1998**, *459*, 135.
(47) Piao, T.; et al. *J. Electrochem. Soc.* **1999**, *146*, 2794.
(48) Kim, Y.-O.; Park, S.-M. *J. Electrochem. Soc.* **2001**, *148*, A194.
(49) Gabrielli, C.; Haas, O.; Takenouti, H. *J. Appl. Electrochem.* **1987**, *17*, 82.
(50) Johnson, B. J.; Park, S.-M. *J. Electrochem. Soc.* **1996**, *143*, 1269.
(51) Lee, J.-Y.; Park, S.-M. *J. Electrochem. Soc.* **2000**, *147*, 4189.
(52) Yoo, J.-S.; et al. *Anal. Chem.* **2003**, *75*, 2962.
(53) Park, S.-M. In *Handbook of Conductive Molecules and Polymers*; Nalwa, H. S., Ed.; Wiley: Chichester, England, 1997; Vol. 3.